

# Chromatin Is Frequently Unknotted at the Megabase Scale

Dimos Goundaroulis,<sup>1,2</sup> Erez Lieberman Aiden,<sup>3,4,\*</sup> and Andrzej Stasiak<sup>1,2,\*</sup>

<sup>1</sup>Center for Integrative Genomics, University of Lausanne, Lausanne, Switzerland; <sup>2</sup>SIB Swiss Institute of Bioinformatics, Lausanne, Switzerland; <sup>3</sup>Center for Genome Architecture, Baylor College of Medicine, Houston, Texas; and <sup>4</sup>Center for Theoretical Biological Physics, Rice University, Houston, Texas

**ABSTRACT** Knots in the human genome would greatly impact diverse cellular processes ranging from transcription to gene regulation. To date, it has not been possible to directly examine the genome in vivo for the presence of knots. Recently, methods for serial fluorescent in situ hybridization have made it possible to measure the three-dimensional position of dozens of consecutive genomic loci in vivo. However, the determination of whether genomic trajectories are knotted remains challenging because small errors in the localization of a single locus can transform an unknotted trajectory into a highly knotted trajectory and vice versa. Here, we use stochastic closure analysis to determine if a genomic trajectory is knotted in the setting of experimental noise. We analyze 4727 deposited genomic trajectories of a 2-Mb-long chromatin interval from human chromosome 21. For 243 of these trajectories, their knottedness could be reliably determined despite the possibility of localization errors. Strikingly, in each of these 243 cases, the trajectory was unknotted. We note a potential source of bias insofar as knotted contours may be more difficult to reliably resolve. Nevertheless, our data are consistent with a model in which, at the scales probed, the human genome is often free of knots.

**SIGNIFICANCE** After cell division, chromosomes decondense and lose their characteristically clearly defined shapes commonly recognized as chromosomes. Yet it is in this decondensed state in which such crucial processes as transcription and DNA replication occur. Until recently, it was broadly assumed that chromatin fibers in decondensed chromosomes behave like randomly fluctuating chains, which in the presence of cellular topoisomerases, freely pass through each other forming knots. However, more recently, proximity ligation assays (Hi-C) indirectly suggested that decondensed chromosomes are unknotted. The recently developed Oligopaint method of serial fluorescent labeling of consecutive short chromatin portions permits one to directly trace individual chromatin fibers along up to 2-million-basepair-long stretches. Here, we analyze Oligopaint chromosome tracings for the presence of knots.

## INTRODUCTION

When freshly divided eukaryotic cells, such as human cells, enter the interphase stage of the cell cycle, their chromosomes decondense and spread within the volume of chromosomal territories (1). Each decondensed chromosome contains one very long chromatin fiber, which in an average-sized human chromosome, contains ~130 million basepairs (2). Because the linear density of chromatin fibers is ~100 bp/nm (3), the length of chromatin fiber of an average chromosome is ~1300  $\mu\text{m}$ . This length is sufficient

to traverse several hundred times across individual chromosome territories, which are roughly spherical and have a diameter of ~2  $\mu\text{m}$  (1). Chromatin fibers in chromosomal territories are associated with DNA topoisomerases that through transient cleavages and relegations can permit interacting regions of chromatin fibers to pass through each other (4,5). Given these considerations, the natural expectation is that chromatin fibers in interphase chromosomes form very complex knots (6). However, studies measuring how the probability of contacts between chromosomal loci decreases with the genomic distance separating these loci exclude the possibility that decondensed chromosomes form such complex knots as could be formed if chromatin fibers could freely pass through each other in topoisomerase-mediated reactions (6). The observed scaling profiles relating contact probability to the genomic distance did not exclude however

Submitted September 25, 2019, and accepted for publication November 5, 2019.

\*Correspondence: [andrzej.stasiak@unil.ch](mailto:andrzej.stasiak@unil.ch) or [erez@erez.com](mailto:erez@erez.com)

Editor: Tamar Schlick.

<https://doi.org/10.1016/j.bpj.2019.11.002>

© 2019 Biophysical Society.

This is an open access article under the CC BY-NC-ND license (<http://creativecommons.org/licenses/by-nc-nd/4.0/>).



the possibility that relatively simple chromatin knots can be scattered within decondensed chromosomes (7).

Because of the linear structure of eukaryotic chromosomes, such unequivocal methods of detection of DNA knots on circular DNA molecules as gel electrophoresis (8–10) or electron microscopy (11,12) cannot be used to directly answer the question of whether interphase human chromosomes are knotted. However, gel electrophoresis can be used to study the formation of knots in circular yeast minichromosomes, which are naturally existing, autonomously replicating, extrachromosomal genetic elements with normal chromatin structure (10). Very recent studies of yeast minichromosomes revealed that as the size of studied yeast minichromosomes increases from 1.4 to 11.7 kb, the steady-state fraction of knots initially increases with the size of minichromosomes but then stabilizes at the value of ~3% upon reaching the size of 8 kb (10). The observation that the probability of knotting of chromatin rings forming minichromosomes does not exceed 3%, irrespectively of the size of circular minichromosomes, suggests that normal yeast chromosomes, with the average size of ~750 kb, may also show a similarly low level of knotting (10). However, the questions of whether chromatin fibers in interphase chromosomes of higher eukaryotes, such as humans, are knotted and what is the frequency of these knots arises. Because crowding of chromatin in cells of higher eukaryotes is stronger than in yeast cells, the equilibrium knotting level could be correspondingly higher.

On the other hand, knotting level in chromatin constituting chromosomes of higher eukaryotes, such as humans, may be much lower than that detected in circular minichromosomes of yeast. Replication of circular DNA molecules encounters particular topological difficulties (13,14), and these topological difficulties were shown to result in the formation of knots in replicating DNA molecules (15–17). Because chromatin fibers in human chromosomes are not circular, the process of their replication may not generate knots.

Indeed, early studies using Hi-C to measure the contact probability between pairs of loci genome wide were consistent with such models of chromatin folding as fractal globule in which knots are absent (6) or models in which knotting is very limited and may consist at most of the simple knots scattered within decondensed chromosomes (7). Also, newer theoretical studies based on Hi-C data showed that block copolymer nature of chromatin, where regions with the same epigenetic marks attract each other, suggested that the presence of knots is thermodynamically disfavored in such a system, as compared to simple self-avoiding homopolymer models of chromatin (18). In addition, the process of chromatin loop extrusion could also provide a very efficient way to unknot chromatin (19,20).

Until recently, there were no methods of structural analysis of entire chromosomes that could permit detection and characterization of individual knots formed on chro-

matin fibers within eukaryotic chromosomes. However, recently, such methods like single-cell Hi-C opened the possibility to reconstruct chromatin paths in individual chromosomes at the moment of cell fixation (21). Previous methods of population Hi-C could only give information about the average path of chromatin fibers constituting a given chromosome in millions of cells of a given type (6,22,23), and because chromosomes are highly dynamic (24), one could not use the population Hi-C data to search for chromatin knots in individual chromosomes. Very recent studies using numerical simulations to analyze single-cell Hi-C data suggested that chromatin fibers in individual chromosomes can be knotted (25–28). However, the concluded knotting level was low with just one trefoil knot that appeared consistently in independent numerical simulations starting from the same single-cell Hi-C data of human chromosome 14 (28). However, the apparent paucity of chromatin knots concluded from single-cell Hi-C data may be the consequence of unavoidable low resolution of the single-cell Hi-C approach that currently does not exceed 100 kb (21). Therefore, in numerical simulations based on single-cell Hi-C data, individual chromosomes are modeled as continuous polygonal chains with each segment representing a 100-kb-large portion of chromatin (25). It is obvious that if there were relatively tight chromatin knots with their average size of ~100 kb, they would not be realizable as knots in chromosomes modeled with 100-kb resolution because they would be represented by just one or two straight segments in modeled chromosomes. However, it is less obvious that to form even a simplest knot using a polygonal chain, one needs at least six segments (29). For this reason, all possible chromatin knots that were not spread over a chromatin portion larger than 500 kb could only form unknotted portions of the polygonal chain representing a given chromosome modeled at 100-kb resolution. In fact, the reproducibly observed trefoil knot in modeling studies based on single-cell Hi-C data was spread over 25 segments, which corresponds to a 2.5-Mb large chromatin portion (25,28).

To probe the knottedness of chromatin at a smaller scale than these probed using the single-cell Hi-C approach, one would need a method that can provide us with the spatial positions of chromatin intervals smaller than 100 kb. Very recently, an exciting new approach has emerged that has combined Oligopaint chromatin labeling with high-resolution optical imaging to determine the position of a series of consecutive loci (30,31). Using this approach, the centroid positions of many sequential 30-kb-large chromatin loci spanning a 2-Mb-long chromosomal region were determined with 50 nm accuracy (30).

Here, we use stochastic closure analysis to determine if genomic trajectories in interphase chromosomes are knotted in the setting of realistic experimental noise. We use our method to look for knots in 4727 chromatin tracings of 2-Mb-large chromosomal regions of chromosome 21 in

cultured human lung fibroblast cell line IMR90. The analyzed chromatin tracings were originally acquired by Bintu et al. (30) in thousands of individual cells and are publicly available at [https://raw.githubusercontent.com/BogdanBintu/ChromatinImaging/master/Data/IMR90\\_chr21-28-30Mb.csv](https://raw.githubusercontent.com/BogdanBintu/ChromatinImaging/master/Data/IMR90_chr21-28-30Mb.csv). In the analyzed cell line, the investigated chromosome region is transcriptionally active as based on epigenetic histone modifications (which positions can be accessed via 3dg.io/spacewalk); this region forms two topologically associated domains (30).

We find that the true topology of the region could be inferred in 243 cases. Strikingly, in each case, we found that the region was unknotted.

## MATERIALS AND METHODS

### Oligopaint chromatin tracing

Here, we analyze chromosome tracings deposited by Bintu et al. (30). The detailed description of the complex Oligopaint method of simultaneous tracing of selected genomic regions in chromosomes within thousands of fixed cells can be found in Bintu et al. (30). Here, we just briefly describe the principle of the method. The Oligopaint method used by Bintu et al. (30) permitted the authors to label one after the other many consecutive 30-kb-long regions of chromatin constituting together a ~2-Mb-large chromatin fragment. Each 30-kb-long chromatin region was hybridized with ~300 fluorescent probes that were practically uniformly redistributed within each 30-kb fragment. A diffraction-limited three-dimensional image of each labeled 30-kb fragment served to determine the  $X$ ,  $Y$ , and  $Z$  coordinates of the centroid position of each region. Once imaging of cells with the first labeled 30-kb fragment was finished, the labeling was removed, the next 30-kb fragment was labeled with another 300 fluorescent probes, and new images were acquired. The procedure was repeated for more than 60 cycles, until the desired regions with up to 2 MB were traced. Control reactions, in which a given region was labeled for the second time, showed that the two experimental localizations of centroid position of the same 30-kb-long chromatin portions differed from each other, but the difference did not exceed 50 nm. Therefore, the precision/error determining spatial positions of sequential 30-kb-long chromatin portions by Oligopaint method is of ~50 nm (30). The tracings of individual 2-Mb-long chromatin regions are represented by polygonal curves in which the sequential vertices are the Oligopaint-determined positions of centroids of consecutive 30-kb-long chromatin regions in a given analyzed chromosome.

### Numerical closure and knot type determination of individual chromosome tracings

Individual polygonal curves determined by  $X$ ,  $Y$ , and  $Z$  coordinates of individual tracings were closed as described earlier (32). In brief, each polygonal curve was closed 100 times by adding each time two very long segments starting from the two end points of the curve and being directed parallel to each other. The closure was completed by adding a straight segment joining the two distal ends of the two long segments. The procedure was repeated 100 times, but each time, the direction of both added parallel long segments was changed. The 100 directions of added long segments were equally redistributed in the space. The knot type resulting from each closing direction was determined by the calculation of Jones (33) and HOMFLY-PT polynomials (34,35). The knot type that was most frequently identified among 100 differently closed curves was then assumed to represent the topology of a given tracing. A similar multiple-closure procedure was used earlier to detect the dominant knot type of simulated chromosomal trajectories (26). In figures and tables, we apply the Alex-

ander-Briggs notation of knots in which the first number indicates the minimal number of crossings a given knot can show in a projection and the second number, written as a subscript, indicates the tabular position of that knot in standard tables of knots among knots with the same number of crossings (36). Thus, for example, the notation  $3_1$  indicates a knot type that in its minimal crossing representation shows three crossings. The subscript 1 indicates that this knot in standard tables of knots is presented at the first position among knots with three crossings, although there is only one knot type with three crossings. However, because the number of possible knot types increases with the number of crossings, the notation  $9_{30}$  indicates a knot type that in standard tables of knots is presented at the 30th position among 49 different prime knots whose minimal crossing number is 9. In the case of knots with more than 10 crossings, the notations include also letters “a” or “n” to indicate whether a given knot is alternating or nonalternating, respectively (37). The notation of composite knots resulting from tying of two or more separate prime knots contains the “#” sign between the corresponding prime knots.

### Topological analysis of all subchains in polygonal chains

Because all subchains in polygonal chains are linear, their topological analysis is performed similarly to the topological analysis of entire chains. Each subchain was subject to a stochastic multiple-closure procedure, and the knot type observed most frequently among closed chains was attributed to a given subchain. The results of topological analysis of all subchains of a given larger chain are conveniently presented as a matrix in which a color of each cell tells us what is the knot type of the subchain that starts with the vertex indicated on the  $X$  axis and ends with the vertex indicated on the  $Y$  axis (38).

### Numerical simulation of topological consequences of the limited precision of tracing procedure

To simulate the effect of a limited precision of the determination of the centroid position of sequential 30-kb-long chromatin blocks, we took coordinates of individual deposited tracings and introduced method-specific tracing errors to positions of every vertex. The new values of  $X$ ,  $Y$ , and  $Z$  coordinates of each vertex were taken from the normal distribution centered at the original position. The normal distribution function along each axis was scaled in such a way that its standard deviation coincided with a 50-nm distance from the original position. In addition, we rejected all trial displacements in which the combinations of displacements along the  $X$ ,  $Y$ , and  $Z$  axis resulted in a three-dimensional displacement from the original point being larger than 50 nm. If a trial displacement was rejected, a new displacement was tested. Using this procedure, for every analyzed tracing, we produced 10 independent tracings in which each 1 was derived from the original deposited tracing. Each error-perturbed tracing was then subject to stochastic multiple closure with 100 closures equally redistributed in space to determine the dominant knot type conditioned by a given error-perturbed tracing. Then, we analyzed whether error-induced perturbations resulted in changes of the knot type as compared to the knot type of the deposited, non-perturbed tracings.

Our testing of the effects of experimental error on the resulting topology of reconstructed chromatin trajectories is conceptually similar to the approach taken by Siebert et al. (25). Siebert et al. (25) did not directly perturb the configurations they obtained in simulations aimed to reproduce Hi-C contact set. However, starting from the same data set, they have repeated the simulations several times. When independent simulations finished, the resulting configurations were somewhat different from each other and they frequently formed different knot types, thus revealing the effect of limited precision of the method on the concluded topology of simulated chromatin fibers.

## RESULTS

### Visualization and analysis of deposited chromosomal tracings

Fig. 1 shows a polygonal chain corresponding to the first deposited tracing (IMR90\_chr21-28-30Mb.csv chr\_idx:1) of  $\sim 2$ -Mb-long chromatin fiber constituting the region 28–30 MB of human chromosome 21, studied by Bintu et al. (30). The sequential vertices of the shown chain correspond to centroid positions of sequential 30-kb-long chromatin portions as determined by Oligopaint chromatin tracing. The diameter of all segments in the chain is set to correspond to the physical diameter of 10 nm because this reflects the diameter of chromatin fibers in interphase chromosomes (39). The two spherical beads placed at the ends of polygonal chains have their diameter set to correspond to a physical distance of 50 nm because this is the reported error range in the determination of the centroid positions of sequential 30-kb-long chromatin regions (30). It is visible that in many places, the nonconsecutive segments of the chain approach each other at a distance much smaller than 50 nm. Therefore, considering the limited precision of the method, one cannot be certain whether the tracing correctly reflects the topology of the traced region. However, the shown tracing, as it is, is topologically characterized as forming  $9_{30}$  knot (see below how the knot type of open polygonal curves is determined here). A standard, minimal crossing representation of that knot is shown in an inset in Fig. 1.

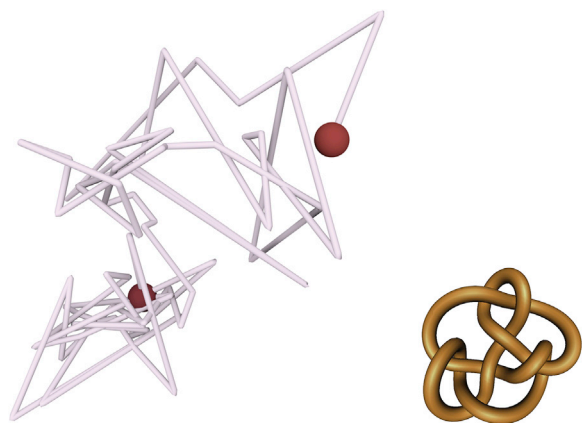


FIGURE 1 Polygonal chain determined by one of the deposited chromatin tracings by Bintu et al. (30). The  $X$ ,  $Y$ , and  $Z$  coordinates of sequential vertices are the coordinates of centroid positions of sequential 30-kb-long chromatin portions as measured using the Oligopaint method (30). The shown polygonal chain corresponds to the tracing IMR90\_chr21-28-30Mb.csv chr\_idx:1; multiple-closure analysis reveals that it forms a  $9_{30}$  knot. The diameter of segments is set to correspond to the physical diameter of 10 nm to reflect the diameter of 10-nm chromatin fibers. The diameter of large beads, placed at both ends of the polygonal chain, is set to 50 nm to reflect the error range in the determination of the position of centroid positions of 30-kb-long chromatin portions using the Oligopaint method. The inset shows a minimal crossing representation of a  $9_{30}$  knot.

### Statistical analysis of the global knottedness of 4272 independently traced 2-Mb-large chromosomal regions

In a strict topological sense, knots can be only defined for closed paths in space. However, individual chromatin fibers forming entire chromosomes in eukaryotic cells are linear, and this of course also applies to traced chromosomal regions analyzed here. To be able to characterize the topology of open paths in space, one needs to close them. However, the process of closure, such as that resulting from adding a segment joining the two ends of a polygonal open curve, can introduce entanglements that were not intrinsic to the analyzed open curve. Various inventive methods of closure were proposed to minimize the influence of closure on the resulting topology of analyzed linear paths (40–45). Unfortunately, in each case, the addition of closing segments changes the geometry of the analyzed path in space. This makes that the resulting knot type is not only conditioned by the geometry of the analyzed open curve but also by the geometry of somewhat arbitrarily chosen construction of the closing part.

To reveal the intrinsic topology of analyzed open curves not affected by a particular set of closing segments, a technique involving multiple stochastic closures was introduced (46,47). In the multiple-closure approach, in which each closure traces a different path, the distorting effects of individual placements of closing segments are averaged out. One method of a multiple stochastic closure of open curves consists of curves' closure at “infinity” along a number of equally redistributed directions radiating from a given point (32). In practice, this method corresponds to adding to each of two ends of the open curve a long segment that is parallel to the other added segment. Once the added segments extend beyond the initial open curve, their ends are joined by a third segment (see Fig. 2 A). The formed closed curve is then characterized with respect to its topology. The closing procedure is then repeated many times, but each time, the two long added segments follow a different direction among many equally redistributed directions radiating from a given point (see Fig. 2 A). In the analysis reported here, we closed each of the analyzed polygonal curves along 100 equally redistributed directions. Importantly, not all directions of closure of a given open curve result in formation of the same knot type, and frequently, many different knot types are formed when the added parallel segments scan 100 different directions of closure (see Fig. 2 B). In the case of the tracing IMR90\_chr21-28-30Mb.csv chr\_idx:1, the  $9_{30}$  knot was observed most frequently among knots resulting from different directions of closure (see Fig. 2 B); therefore, knot  $9_{30}$  is assumed here to represent most closely the topology of the deposited tracing that is shown in Fig. 1.

We then extended this type of topological analysis to thousands of deposited tracings of the same 2-Mb-large chromosome regions of chromosome 21 but acquired in

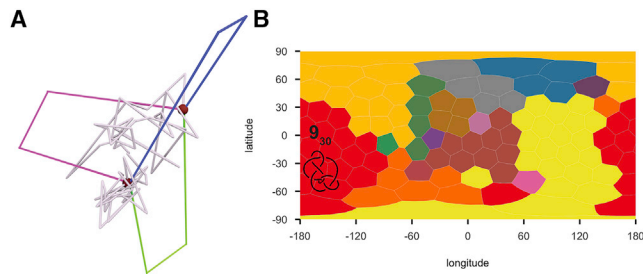


**FIGURE 2** The multiple-closure approach reveals the intrinsic topology of an open curve. (A) Pairs of long segments, which in each case were parallel to each other, were added to both ends of the analyzed tracing. Once the added segments extended beyond the analyzed polygonal chain, they were connected with an additional segment, thus forming a closed curve, which knot type can be formally characterized from. Different colors of added segments show individual closures. Each analyzed tracing was closed 100 times where the directions of added parallel segments were uniformly distributed in the unit sphere. (B) 100 directions of closures and the resulting knot types are shown. A map representation showing how the closure direction affects the formed knot type is shown. Different colors of Voronoi cells indicate different knot types resulting from the closures in which the added parallel segments were oriented along an indicated latitude and longitude angle. In the shown case, the most frequently observed (23%) knot type was the  $9_{30}$  knot, although several other individual knot types were also observed in slightly smaller fractions of closures. Notice however that the shown graphs/maps do not preserve the surface of the spheres they represent and the area of individual Voronoi cells, corresponding to the given direction of closure, which increases as the latitude angle increases. Notice also that the shown maps are periodic in horizontal direction; therefore, the knot territories adjacent to the left and right border of the map are in fact contiguous with each other. Knot type notation of the most frequently observed knot type is indicated on corresponding “knot countries.” In addition, the diagram of the most frequently observed knot type is also shown. In the matrix shown in (B) and in matrices shown in Figs. 3, 4, 5, and 6, the red color is used to indicate knot countries corresponding to the most frequently observed knot type conditioned by a given polygonal curve. Indicating the knot types of other knot countries turned out to be impractical because these countries are only intended to show that depending on the closure direction, one can obtain many different knot types starting from the same polygonal chain.

parallel in several thousands of Oligopaint-stained IMR90 cells. Tables 1 and 2 present the statistics of the observed prime and composite knot types, respectively. Out of deposited 4871 tracings, we rejected 143 noncomplete tracings, in which positions of 15 or more out of 65 sequential 30-kb-long chromatin fibers were not determined. In Tables 1 and 2, we only list the knot types that were observed at least 6 times in the analyzed sample of 4727 of independent tracings. Interestingly, with respect to their topology, the deposited tracings behaved similarly to random walks with a moderate size, for which the frequency of forming a given knot is inversely correlated with its complexity (48–52). The majority of analyzed tracings were unknotted (i.e., they formed a trivial knot that has the Alexander-Briggs notation  $0_1$ ). Among nontrivial knots, trefoil knots ( $3_1$ ) were most frequently observed. These were followed then by so-called figure-eight knots that are knots having only four crossings ( $4_1$ ), and these were followed by two knots with five crossings, where twist knots  $5_2$  were more frequently

**TABLE 1 Prime Knots Observed in 4727 Deposited Chromatin Tracings of 2-Mb Regions of Chromosome 21 in Thousands of Cultured Human Cells**

Knot	Counts	Frequency
$0_1$	2292	0.4849
$3_1$	929	0.1965
$4_1$	257	0.0544
$5_2$	134	0.0283
$5_1$	69	0.0146
$6_1$	58	0.0123
$6_2$	56	0.0118
$6_3$	33	0.0070
$7_6$	24	0.0050
$8_{20}$	14	0.0030
$7_7$	13	0.0028
$7_2$	9	0.0019
$7_5$	9	0.0019
$7_3$	8	0.0017
$9_{45}$	8	0.0017
$8_{21}$	7	0.0015
$9_{42}$	7	0.0015
$8_4$	6	0.0013
$8_8$	6	0.0013
$8_{10}$	6	0.0013

observed than the torus knots  $5_1$ . That predominance of five crossing twist knots over five crossing torus knots was previously observed in studies of random knots (51,52). Among composite knots with two component knots, the most frequent are those composed of two trefoils ( $3_1\#3_1$ ), and these are followed by those composed of one trefoil knot and one figure-eight knot ( $3_1\#4_1$ ), which in turn are followed by  $3_1\#5_2$ , as could be expected from the probability of formation of corresponding prime knots. Among composite knots with three component knots, the most frequent are those for which each component was a trefoil knot ( $3_1\#3_1\#3_1$ ).

Also, differences in overall dimensions between polygonal tracings forming knots and unknots resembled the situation observed for random walks in which the random walks forming knots had a smaller radius of gyration than random walks forming unknots (53). Our analysis of

**TABLE 2 Composite Knots, That Is, Knots Composed of Two or More Knots Formed on the Same Polygonal Chain, That Were Observed in 4727 Deposited Chromatin Tracings of 2-Mb Regions of Chromosome 21 in Thousands of Cultured Human Cells**

Knot	Counts	Frequency
$3_1\#3_1$	157	0.0332
$3_1\#4_1$	73	0.0154
$3_1\#5_2$	32	0.0068
$3_1\#6_3$	14	0.0030
$3_1\#5_1$	13	0.0028
$3_1\#6_2$	13	0.0028
$3_1\#6_1$	11	0.0025
$4_1\#5_2$	8	0.0023
$3_1\#3_1\#3_1$	7	0.0015
$3_1\#3_1\#4_1$	6	0.0013

tracings forming knots or unknots show that their mean radii of gyration were  $437 \pm 2$  and  $456 \pm 2$  nm, respectively.

If we consider individual tracings forming polygonal chains with 65 segments as random walks, we can see that their frequency of knotting is roughly two times higher than in simulated nonconfined phantom polygonal chains with the corresponding number of segments (50). The higher probability of knotting in polygonal tracings as compared to unconfined polygonal chains, with the same number of segments, indicates that the tracings form spatially confined walks because confinement of random walks increases their knotting probability (54).

### Testing the authenticity of detected nontrivial knots

Although nearly half of the analyzed chromosome tracings were knotted (see Table 1), the question arises of whether these knots are genuine or are the result of the limited precision in the determination of the path of crowded chromatin fibers. Bintu et al. (30) estimated that the error of determination of the centroid position of each 30-kb-large portion of chromatin fiber is  $\sim 50$  nm (30). The diameter of chromatin fiber is  $\sim 10$  nm (39); therefore, a 50-nm error in the determination of paths of crowded chromatin fibers may result in polygonal tracings that are knotted despite the fact that the traced chromatin was in fact unknotted. Also, the opposite could have happened.

To consider whether the knots reported in Table 1 are genuine, let us first perform a thought experiment. Let us assume that we trace highly crowded polymeric chains using a method that gives us an error of tracing that is larger than many shortest distances between approaching each other nonsequential regions of the traced polymeric chain. Let us consider now that the crowded polymeric chain that we trace is in fact unknotted. A little thought tells us that under such circumstances, the produced tracing is very likely to be knotted despite the fact that the traced chain was unknotted. Let us consider now that the crowded polymeric chain that we trace is in fact knotted and forms a simple knot. Another little thought tells us now that the produced tracing will be likely still knotted and possibly even more knotted than before. The chance that an error of tracing of crowded polymeric chain that is knotted would produce an unknot is small. The much larger chance that an error-prone tracing of a crowded path will introduce a knot rather than remove a knot has a very simple explanation. There is an infinite number of various knots and just one trivial knot. Therefore, if we cram an earphone set into a pocket, it is very likely that it will get knotted. However, such a knotted earphone set will not likely become unknotted if we cram it again in the pocket. However, from time to time, this may also happen.

After this thought experiment, we decided to numerically test the effect of tracing errors on the resulting topol-

ogy of produced tracings. We first took the same chromatin tracing that is shown in Fig. 1 and for which multiple-closure analysis is shown in Fig. 2. We took the original tracing and introduced perturbations mimicking the experimental error range of the method, that is, we displaced the position of every vertex by up to 50 nm, as described in the Materials and Methods. We performed this procedure 10 times during which each time, the error-induced perturbations were not correlated with each other but applied randomly. In our analysis of error effects on the detection of chromatin knots, we were inspired by somewhat similar analysis of 10 independent chromosome structure reconstructions from the same single-cell Hi-C data (25). For each of the 10 error-affected configurations, we performed multiple-closure analyses whose results are shown in Fig. 3. It is visible that upon perturbations that mimic the intrinsic experimental error, the deposited tracing that was originally forming a  $9_{30}$  knot gets very frequently converted into other knots. None of the error-perturbed configurations still formed the  $9_{30}$  knot. Three of the error-perturbed configurations formed more complex knots than the unperturbed tracing and were characterized as knots with 10, 11, and more than 12 crossings, respectively. Five of the error-perturbed configurations formed simpler knots than the unperturbed tracing and resulted in knots with eight, seven, six, five, and four crossings, respectively. Interestingly, two of the error-perturbed configurations resulted in a formation of unknotted configuration.

The analysis presented in Fig. 3 indicates that the limited precision of the Oligopaint method makes it an unreliable way of determination of chromatin topology for such compact chromatin paths as shown in Fig. 1. Our observation that 2 out of 10 error-perturbed configurations resulted in the formation of unknotted configurations shows that the deposited knotted tracing is within an error range to a configuration that is unknotted. This latter conclusion is consistent with the notion that traced chromatin fibers may be unknotted and that the knotted character of their tracing is the consequences of the limited precision of the Oligopaint method when applied to crowded chromatin fibers.

### Testing the topological robustness of unknotted tracings

After investigating the effect of experimental errors on the topology of deposited tracings that were classified as knotted, we extended our analysis to tracings that were classified as unknotted. Fig. 4 A shows one of the analyzed chromosomal tracings that was originally classified as unknotted (IMR90\_chr21-28-30Mb.csv chr\_idx:209). That tracing is less compact than the knotted tracing shown in Fig. 1. For this reason, error-induced perturbations capable of displacing individual vertices by up to a 50-nm distance

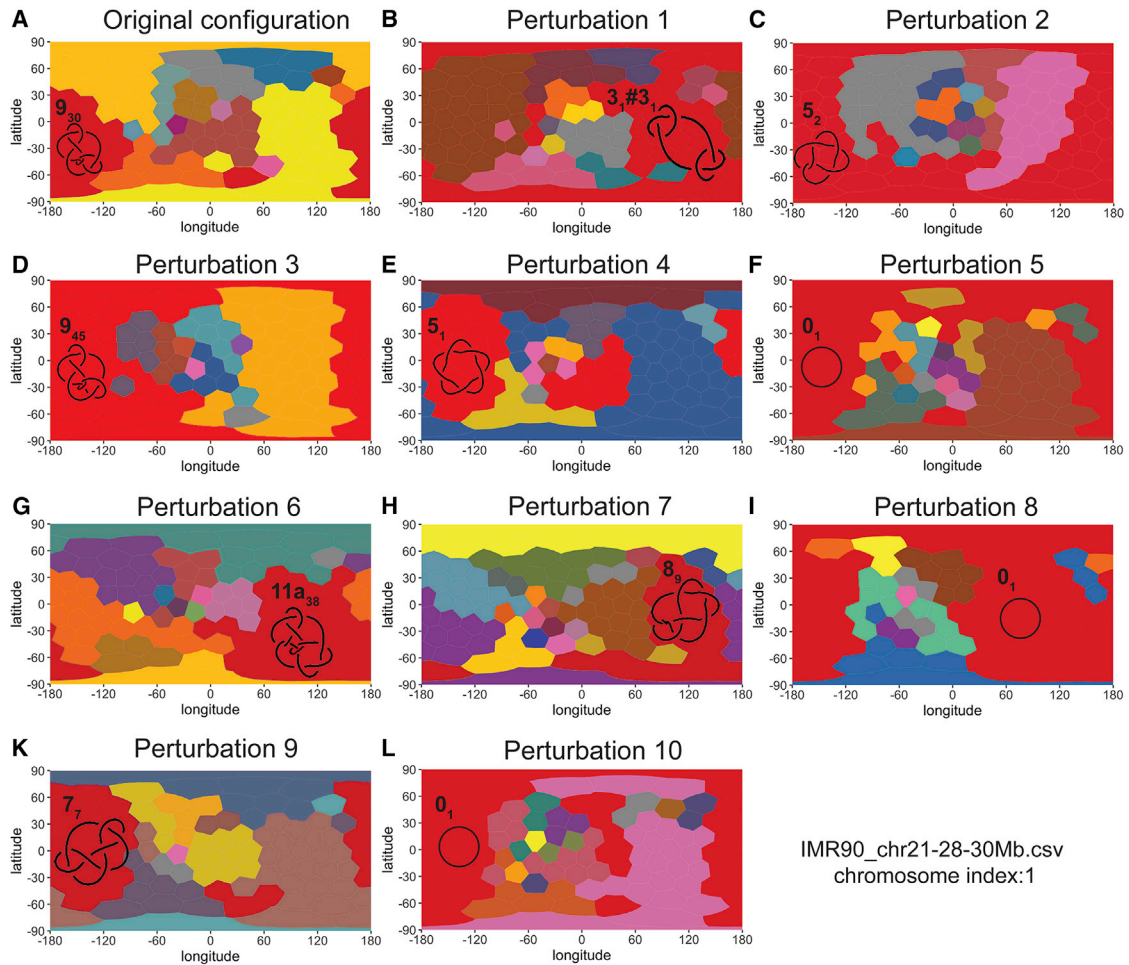


FIGURE 3 Multiple-closure analysis of 10 independently generated error-perturbed configurations of the tracing shown in Fig. 1 and analyzed in Fig. 2. (A) shows the analysis of the original deposited tracing `IMR90_chr21-28-30Mb.csv chr_idx:1`. (B)–(L) show the closure direction maps for 10 error-perturbed configurations derived from the deposited tracing. Notice that perturbations mimicking the effect of limited experimental precision result in a frequent change of the knot type allocated to a given configuration (i.e., the knot type observed for the majority of closure directions). Notice also that three of the error-perturbed configurations (F, I, and L) become unknotted because the majority of their closing directions results in unknots. For each analyzed polygonal curve, the knot type notation of the most frequently observed knot type is indicated on corresponding knot countries. In addition, the diagram of the most frequently observed knot type is also shown. In each map, the red color is chosen to indicate Voronoi cells corresponding to directions of closure that result in the formation of the most frequently observed knot conditioned by a given configuration. The notation and the diagram of the most frequently observed knot, including the trivial knot, is shown in each case.

are unlikely to produce a knotted path out of such a polygonal curve. Fig. 4, B–M show how error-induced perturbations affect the topology of this originally unknotted tracing. The original and all 10 of the error-perturbed configurations form unknots for the great majority of closure directions. Therefore, the unknotted tracing (`IMR90_chr21-28-30Mb.csv chr_idx:209`) can be considered as robustly unknotted.

We extended this type of analysis to all tracings that were classified as unknotted. Among 2292 tracings that were unknotted, 243 were robustly unknotted. Because robustly unknotted tracings are very unlikely to result from an error of tracing method, we can conclude that robustly unknotted tracings correctly report the underlying topology of traced chromatin fibers.

### Search for robust knots

Although we presented earlier arguments that a limited precision of tracing of unknotted but crowded chromatin fibers can easily result in producing knotted tracings, it is also possible that some of the traced chromatin fibers were in fact knotted.

We decided therefore to search for robust knots among the analyzed tracings. Tracings of robust knots should have the property that the knot type detected in them should resist error-induced perturbation, that is, that all of the error-perturbed tracings derived from a given deposited tracing should show the same knot type. Knotted tracings with such a characteristic would be unlikely to result from experimental imprecisions in tracing procedure. Our search for

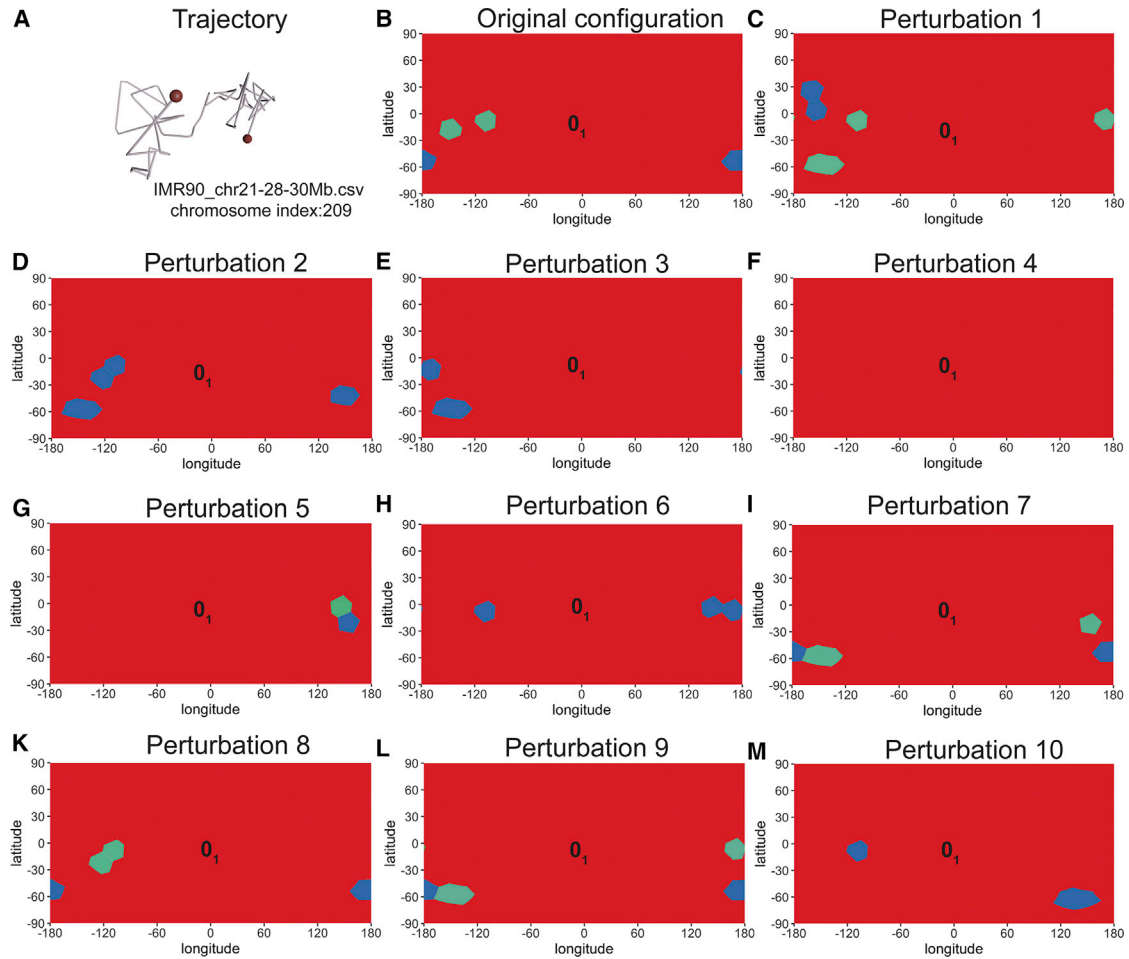


**FIGURE 4** Multiple-closure analysis of an unknotted tracing that is robustly unknotted. (A) shows a polygonal chain corresponding to the deposited tracing IMR90\_chr21-28-30Mb.csv chr\_idx:209. As in Figs. 1 and 2, the diameter of the chain is set to correspond to the physical distance of 10 nm. The two beads at the ends have the diameter corresponding to a physical distance of 50 nm because this is the reported precision of Oligopaint chromatin tracing. (B)–(L) show map representations reporting the type of knots resulting from different directions of closure of unperturbed tracing (B) and 10 error-perturbed configurations derived from unperturbed tracing (C–M). Notice that the unperturbed and also all error-perturbed configurations are unknotted because the majority of closure directions closes them into unknots.

robustly knotted configurations among 509 tracings classified as trefoil knots was not successful. However, we did find several fairly robust configurations, which we defined as those keeping their original knot type in more than 50% of the error-perturbed configurations. Fig. 5 shows one of these fairly robust tracings forming a trefoil knot ( $3_1$ ) together with multiple-closure analysis of its original tracing and 10 error-perturbed tracings. It is visible that 6 out of 10 error-perturbed configurations maintained the knot type of unperturbed tracing. However, 4 out of 10 error-perturbed configurations converted to unknots. This latter observation shows that even such fairly robust tracings forming a trefoil knot can easily be caused by method-specific errors in tracing of unknotted chromatin fibers.

It is important to realize that the search for robust knots cannot be simply done by eliminating all tracings that have no pairs of nonconsecutive segments approaching each other at a distance smaller than 50 nm. On one hand,

such a search would eliminate many trajectories that are potentially topologically robust because not every intersegmental passage results in a change of topology. All passages that introduce or remove nugatory crossings do not change the knot type. On the other hand, polygonal chains that have no pairs of segments getting closer than 50 nm can change their topology upon perturbations. This is caused by the fact that in each perturbation phase, all vertices are moved by up to 50 nm from their original position, and the movement directions are not correlated with each other. Therefore, there is a small probability of having a combination of displacements of vertices that can result in an intersegmental passage of two segments that were originally even as far from each other as nearly 100 nm.

The knot interconversions resulting from error-mimicking perturbations are frequently between knots that require more than one intersegmental passage to pass from one knot to the other. For example, the passage from a  $3_1$

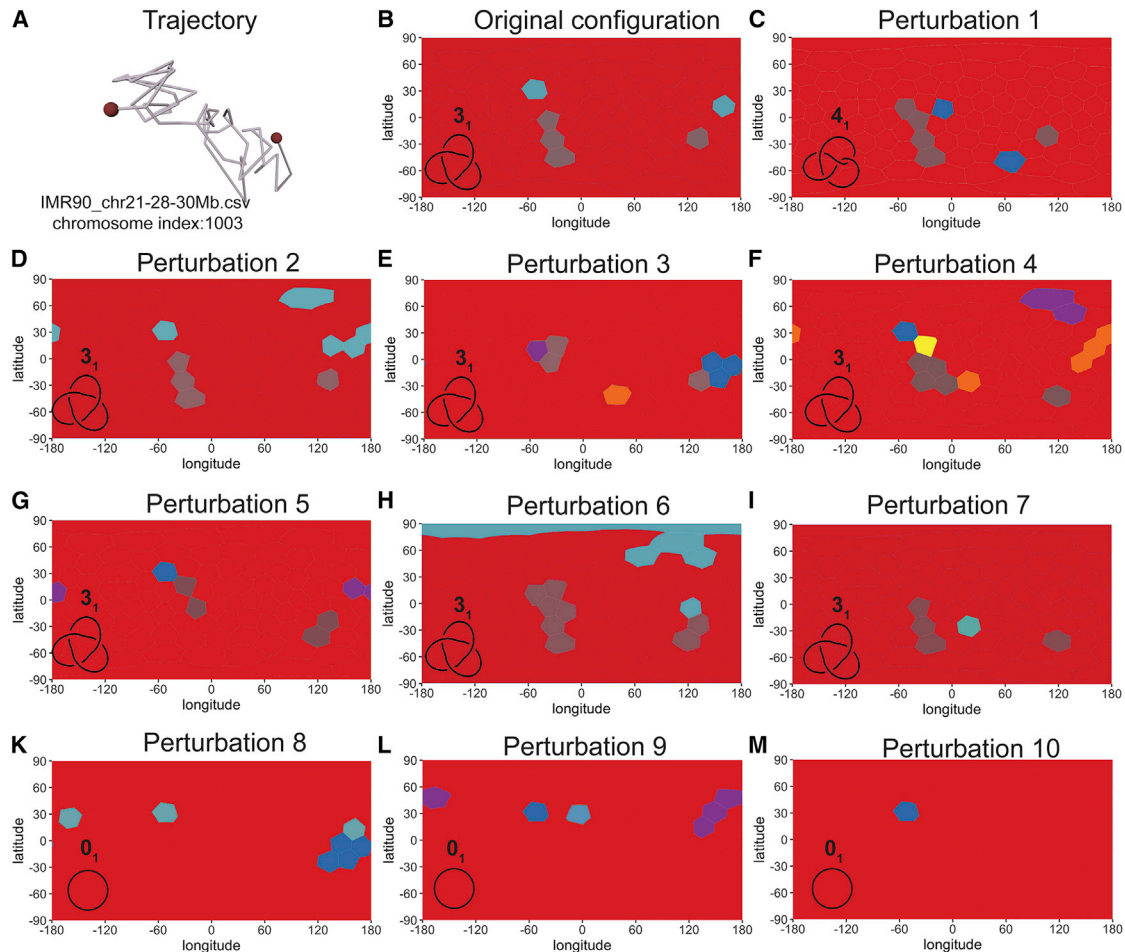


FIGURE 5 Multiple-closure analysis of a fairly robust trefoil-forming tracing. (A) shows a polygonal chain corresponding to the deposited tracing IMR90\_chr21-28-30Mb.csv chr\_idx:1003. (B)–(M) show map representations reporting the type of knots resulting from different directions of closure of unperturbed tracing (B) and 10 error-perturbed configurations derived from unperturbed tracing (C–M). Notice that the unperturbed tracing and also six of the error-perturbed configurations are classified as forming the  $3_1$  knot because the majority of closure directions closes them into the  $3_1$  knot. However, four of the error-perturbed tracings are classified as unknotted.

to  $4_1$  knot, which is documented in Fig. 5 (perturbation 1), requires at least two intersegmental passages (55,56). Such knot interconversions that require two or more intersegmental passages are expected during perturbations in which all vertices are moved in noncorrelated directions and thus are able to result in multiple intersegmental passages.

### Error-mimicking perturbations maintain the position of the knotted core as long as the knot is still present

To provide more insight into the question of whether some of the deposited tracings characterized as fairly robustly knotted correctly report the topology of traced chromatin fibers, we analyzed the position of the knotted core in these configurations. The matrix presented in Fig. 6 A reports the topology of every subchain of the polygonal chain shown in Fig. 5 A. The color of each cell tells us what the knot type of the subchain is that starts with the vertex indi-

cated on the X axis and ends with the vertex indicated on the Y axis (44). The color of the cell in the lower left corner of the matrix indicates the knot type of the entire chain which, in this case, is the  $3_1$  knot. We can also see that the smallest subchain that still forms a  $3_1$  knot and thus forms the knotted core of the chain starts with vertex 17 and ends with vertex 34. Fig. 5, B–L show the topological analysis of subchains in error-perturbed tracings that were analyzed as entire chains in Fig. 5. Interestingly, when error-perturbed configurations are still knotted, they maintain practically the same position of their knotted core as in the unperturbed configuration. Of course, when error-perturbed configurations get unknotted, they do not have any more their knotted core. Error-perturbed tracings shown in Fig. 5, I and K are unknotted when analyzed as entire chains; however, they form slip-knots, and thus some of their subchains form trefoil knots. Fig. 5 M shows a superposition of all 10 matrices shown in Fig. 5, A–L. Such a superposition permits us to visualize more clearly the most persistent patterns.

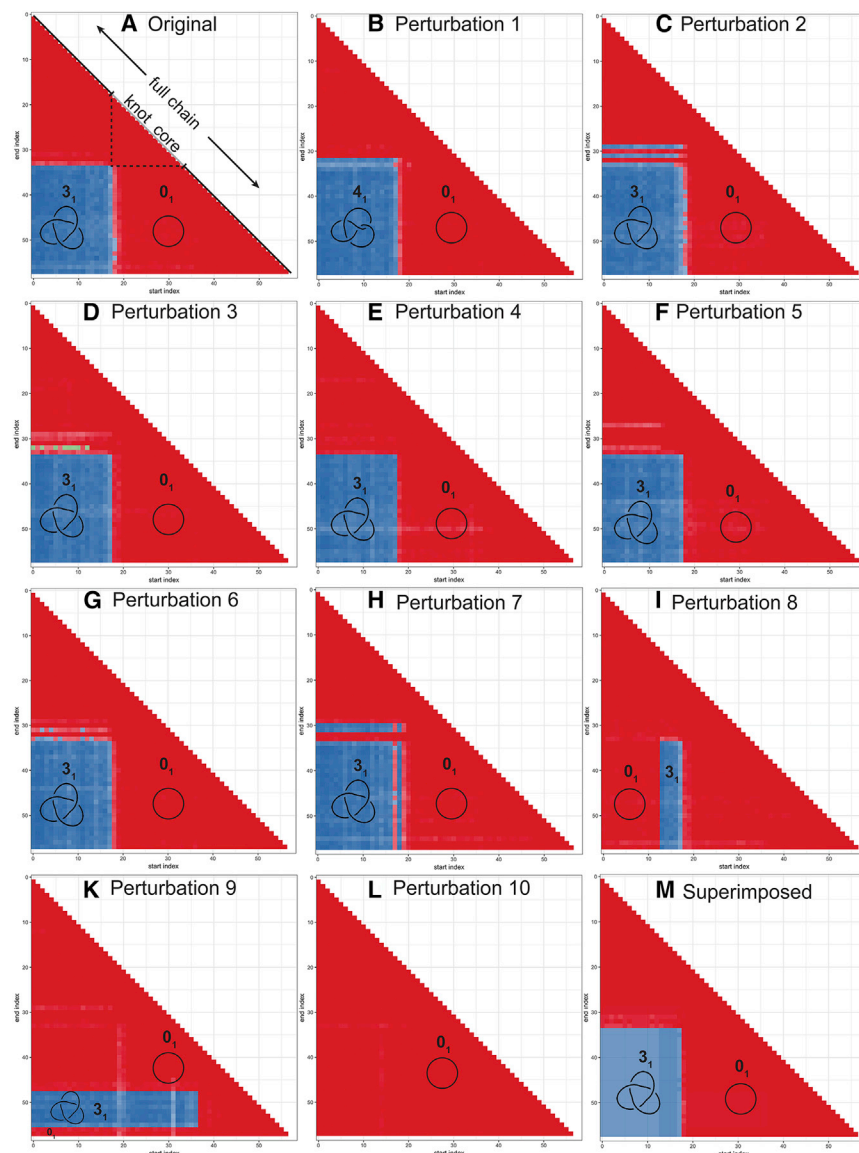


FIGURE 6 Topological characterization of all subchains in the deposited tracing IMR90\_chr21-28-30Mb.csv chr\_idx:1003 that forms a fairly robust trefoil knot (A) and in its error-perturbed configurations (B–M). Colors of individual cells in the matrices (A)–(L) indicate the knot type determined by a subchain; the starting and ending vertices of the subchains are indicated on the X and Y axis, respectively. The knot type of each subchain is determined by the multiple-closure approach presented in Fig. 2 but applied to a given subchain. In each matrix, the cell in the lower left corner represents the entire chain, and its color indicates the corresponding knot type. (A) shows that when the deposited tracing is trimmed beyond vertex 18 from the start or beyond the vertex 33 from the end, the truncated tracing becomes unknotted ( $0_1$ ). Therefore, the core of the knot in this tracing is located between vertices 18 and 33, as additionally illustrated in (A). The matrix shown in (M) is a superposition of matrices shown in (A)–(L).

The presented analysis of effects of perturbation on the location of the knotted core showed that segments delimiting the knotted core do not need to be particularly close to each other. The observation that the position of the knotted core did not move when the original trefoil knot transitioned into a  $4_1$  knot or to a slipknot indicated that passages that are most likely to occur between segment pairs closest to each other occurred in fact in other locations.

## DISCUSSION

Strikingly, despite the fact that the majority of the 4727 deposited chromosome tracings that we analyzed were knotted, it is far from certain that any of the true, underlying 2-Mb-long chromatin fibers were indeed knotted. In fact, we found that measurement errors in the chromosome tracing procedure were sufficient to obfuscate the true

topology in all deposited tracings that were classified as knotted. In all those tracings, the measured topology was not robust to the translation of individual points by distances smaller than the reported error (50 nm) (30). When traced chromatin fibers are highly crowded, as is frequently the case of interphase chromosomes, the errors of this magnitude can easily produce knotted tracings even if the true trajectory of traced chromatin fibers were in fact unknotted. Presumably for this reason, Bintu et al. (30) did not analyze the topology of chromatin tracings deposited by them.

However, it is also possible that analyzed chromatin fibers were in fact knotted. To resolve this ambiguity, we searched for arguments that could tell us whether the observed knots were genuine or artifactual.

The observed spectrum of knots very much resembles the simulated spectra of knotting resulting from topological

equilibration that would be expected to occur in crowded chromatin in vivo if topoisomerases were able to permit free passages of chromatin fibers through each other in living cells (52). However, essentially the same spectrum of knots would be expected if errors of tracings were “transforming” unknotted but compact chromatin paths into knotted paths of their tracings.

An argument that may be interpreted as pointing toward the notion that in vivo chromatin is mainly unknotted was provided however by the absence of robustly knotted tracings (i.e., tracings in which nonconsecutive segments do not approach each other over a distance smaller than 50 nm). The presence of such tracings would provide very strong arguments for the presence of knots in chromatin because such tracings would be very unlikely to result from errors in determination of spatial position of sequentially labeled chromatin portions.

However, we detected 243 tracings that were robustly unknotted, that is, tracings that were very unlikely to result from the tracing of knotted chromatin fibers. Therefore, in all these cases in which tracings had characteristics of correctly reporting the underlying topology of traced chromatin fibers, the analyzed 2-Mb-long chromatin fibers were unknotted.

Crucially, when we use experimental data informing us about centroid positions of sequential 30-kb-long chromatin loci within a 2-Mb-long chromosomal region, we can only detect chromatin knots whose core length is larger than 150 kb and smaller than 2 Mb. This is because at least five segments of polygonal curve are needed to define a knot upon simple closure (29), and each segment in analyzed polygonal tracings corresponds to 30-kb-long chromatin portions. Therefore, if there were chromatin knots with cores smaller than 150 kb, they would not produce knotted parts of polygonal tracings and thus would be missed. However, this compares favorably with the single-cell Hi-C modeling approach, which because of its 100-kb resolution (25–28), could not detect chromatin knots even if they were as large as 500 kb. On the other end of the scale, if the knot core were larger than 2 Mb (the size of analyzed fragments), we would also miss it in our analysis. To not miss larger knots, the Oligopaint method would need to be applied to trace chromatin fibers over a larger length.

A more definite conclusion about whether chromatin in chromosomes is typically knotted will require improvements in the accuracy of chromosome tracings sufficient to enable topological robustness of the resulting trajectories despite crowded conditions. Until then, the problem will remain knotty.

## AUTHOR CONTRIBUTIONS

A.S. and E.L.A. conceived the study. D.G. performed the research. A.S., E.L.A., and D.G. discussed the results and wrote the manuscript.

## ACKNOWLEDGMENTS

We thank all the authors of Bintu et al. (30) for making all chromatin tracings analyzed in this work publicly available. The authors acknowledge the contribution of the COST action EUTOPIA (CA17139).

This work was supported by the Leverhulme Trust (RP2013-K-017 to A.S.), National Science Foundation Physics Frontiers Center award (PHY1427654 to E.L.A.), Welch Foundation (Q-1866 to E.L.A.), US Department of Agriculture Agriculture and Food Research Initiative grant (2017-05741 to E.L.A.), National Institutes of Health 4D Nucleome Program grant (U01HL130010 to E.L.A.), and the National Institutes of Health Encyclopedia of DNA Elements award (UM1HG009375 to E.L.A.).

## REFERENCES

1. Meaburn, K. J., and T. Misteli. 2007. Cell biology: chromosome territories. *Nature*. 445:379–781.
2. Brown, T. A. 2002. *Genomes*, Second Edition. Wiley-Liss, Garland Science, Oxford, UK.
3. Papale, A., and A. Rosa. 2019. Structure and microrheology of genome organization: from experiments to physical modelling. In *Modeling the 3D Conformation of Genomes*. G. Tiana and L. Giorgetti, eds. CRC Press, pp. 139–176.
4. Pommier, Y., Y. Sun, ..., J. L. Nitiss. 2016. Roles of eukaryotic topoisomerases in transcription, replication and genomic stability. *Nat. Rev. Mol. Cell Biol.* 17:703–721.
5. Björkegren, C., and L. Baranello. 2018. DNA supercoiling, topoisomerases, and cohesin: partners in regulating chromatin architecture? *Int. J. Mol. Sci.* 19:E884.
6. Lieberman-Aiden, E., N. L. van Berkum, ..., J. Dekker. 2009. Comprehensive mapping of long-range interactions reveals folding principles of the human genome. *Science*. 326:289–293.
7. Arsuaga, J., R. G. Jayasinghe, ..., M. Vazquez. 2015. Current theoretical models fail to predict the topological complexity of the human genome. *Front. Mol. Biosci.* 2:48.
8. Crisona, N. J., R. Kanaar, ..., N. R. Cozzarelli. 1994. Processive recombination by wild-type gin and an enhancer-independent mutant. Insight into the mechanisms of recombination selectivity and strand exchange. *J. Mol. Biol.* 243:437–457.
9. Schwartzman, J. B., M. L. Martínez-Robles, ..., D. B. Krimer. 2013. Plasmid DNA topology assayed by two-dimensional agarose gel electrophoresis. *Methods Mol. Biol.* 1054:121–132.
10. Valdés, A., J. Segura, ..., J. Roca. 2018. DNA knots occur in intracellular chromatin. *Nucleic Acids Res.* 46:650–660.
11. Krasnow, M. A., A. Stasiak, ..., N. R. Cozzarelli. 1983. Determination of the absolute handedness of knots and catenanes of DNA. *Nature*. 304:559–560.
12. Wasserman, S. A., J. M. Dungan, and N. R. Cozzarelli. 1985. Discovery of a predicted DNA knot substantiates a model for site-specific recombination. *Science*. 229:171–174.
13. Sundin, O., and A. Varshavsky. 1980. Terminal stages of SV40 DNA replication proceed via multiply intertwined catenated dimers. *Cell*. 21:103–114.
14. Laurie, B., V. Katritch, ..., A. Stasiak. 1998. Geometry and physics of catenanes applied to the study of DNA replication. *Biophys. J.* 74:2815–2822.
15. Olavarrieta, L., M. L. Martínez-Robles, ..., J. B. Schwartzman. 2002. Supercoiling, knotting and replication fork reversal in partially replicated plasmids. *Nucleic Acids Res.* 30:656–666.
16. O’Donnell, D., A. Stasiak, and D. Buck. 2018. Two convergent pathways of DNA knotting in replicating DNA molecules as revealed by  $\theta$ -curve analysis. *Nucleic Acids Res.* 46:9181–9188.

17. Schwartzman, J. B., P. Hernández, ..., A. Stasiak. 2019. Closing the DNA replication cycle: from simple circular molecules to supercoiled and knotted DNA catenanes. *Nucleic Acids Res.* 47:7182–7198.
18. Di Pierro, M., B. Zhang, ..., J. N. Onuchic. 2016. Transferable model for chromosome architecture. *Proc. Natl. Acad. Sci. USA.* 113:12168–12173.
19. Racko, D., F. Benedetti, ..., A. Stasiak. 2018. Chromatin loop extrusion and chromatin unknotting. *Polymers (Basel).* 10:E1126.
20. Orlandini, E., D. Marenduzzo, and D. Michieletto. 2019. Synergy of topoisomerase and structural-maintenance-of-chromosomes proteins creates a universal pathway to simplify genome topology. *Proc. Natl. Acad. Sci. USA.* 116:8149–8154.
21. Stevens, T. J., D. Lando, ..., E. D. Laue. 2017. 3D structures of individual mammalian genomes studied by single-cell Hi-C. *Nature.* 544:59–64.
22. Dixon, J. R., S. Selvaraj, ..., B. Ren. 2012. Topological domains in mammalian genomes identified by analysis of chromatin interactions. *Nature.* 485:376–380.
23. Rao, S. S., M. H. Huntley, ..., E. L. Aiden. 2014. A 3D map of the human genome at kilobase resolution reveals principles of chromatin looping. *Cell.* 159:1665–1680.
24. Gasser, S. M. 2002. Visualizing chromatin dynamics in interphase nuclei. *Science.* 296:1412–1416.
25. Siebert, J. T., A. N. Kivel, ..., P. Virnau. 2017. Are there knots in chromosomes? *Polymers (Basel).* 9:E317.
26. Sulkowska, J. I., S. Niewieczeral, ..., W. Niemyska. 2018. KnotGenome: a server to analyze entanglements of chromosomes. *Nucleic Acids Res.* 46:W17–W24.
27. Niewieczeral, S., W. Niemyska, and J. I. Sulkowska. 2019. Defining and detecting links in chromosomes. *Sci. Rep.* 9:11753.
28. Wettermann, S., M. Brems, ..., P. Virnau. 2019. A minimal Gō-model for rebuilding whole genome structures from haploid single-cell Hi-C data. *Comput. Mater. Sci* Published online November 5, 2019. <https://doi.org/10.1016/j.commatsci.2019.109178>.
29. Calvo, J. A., and K. C. Millett. 1998. Minimal edge piecewise linear knots. In *Series on Knots and Everything: Ideal Knots*. A. Stasiak, V. Katritch, and L. H. Kauffman, eds. World Scientific, pp. 107–128.
30. Bintu, B., L. J. Mateo, ..., X. Zhuang. 2018. Super-resolution chromatin tracing reveals domains and cooperative interactions in single cells. *Science.* 362:eaau1783.
31. Nir, G., I. Farabella, ..., C. T. Wu. 2018. Walking along chromosomes with super-resolution imaging, contact maps, and integrative modeling. *PLoS Genet.* 14:e1007872.
32. Dorier, J., D. Goundaroulis, ..., A. Stasiak. 2018. Knoto-ID: a tool to study the entanglement of open protein chains using the concept of knotoids. *Bioinformatics.* 34:3402–3404.
33. Jones, V. F. R. 1987. Hecke algebra representations of braid groups and link polynomials. *Ann. Math.* 126:335–388.
34. Freyd, P., D. Yetter, ..., A. Ocneanu. 1985. A new polynomial invariant of knots and links. *Bull. Am. Math. Soc.* 12:239–246.
35. Przytycki, J. H., and P. Traczyk. 1988. Invariants of links of conway type. *Kobe J. Math.* 4:115–139.
36. Adams, C. C. 1994. *The Knot Book*. W.H. Freeman and Company, New York.
37. Hoste, J., M. Thistlethwaite, and J. Weeks. 1998. The first 1,701,935 knots. *Math. Intell.* 20:33–48.
38. Sułkowska, J. I., E. J. Rawdon, ..., A. Stasiak. 2012. Conservation of complex knotting and slipknotting patterns in proteins. *Proc. Natl. Acad. Sci. USA.* 109:E1715–E1723.
39. Hansen, J. C., M. Connolly, ..., K. Maeshima. 2018. The 10-nm chromatin fiber and its relationship to interphase chromosome organization. *Biochem. Soc. Trans.* 46:67–76.
40. Janse van Rensburg, E. J., D. A. W. Sumners, ..., S. G. Whittington. 1992. Entanglement complexity of self-avoiding walks. *J. Phys. Math. Gen.* 25:6557–6566.
41. Marcone, B., E. Orlandini, ..., F. Zonta. 2005. What is the length of a knot in a polymer? *J. Phys. Math. Gen.* 38:L15–L21.
42. Virnau, P., L. A. Mirny, and M. Kardar. 2006. Intricate knots in proteins: function and evolution. *PLoS Comput. Biol.* 2:e122.
43. Lua, R. C., and A. Y. Grosberg. 2006. Statistics of knots, geometry of conformations, and evolution of proteins. *PLoS Comput. Biol.* 2:e45.
44. King, N. P., E. O. Yeates, and T. O. Yeates. 2007. Identification of rare slipknots in proteins and their implications for stability and folding. *J. Mol. Biol.* 373:153–166.
45. Tubiana, L., E. Orlandini, and C. Micheletti. 2011. Probing the entanglement and locating knots in ring polymers: a comparative study of different arc closure schemes. *Prog. Theor. Phys. Suppl.* 191:192–204.
46. Mansfield, M. L. 1994. Are there knots in proteins? *Nat. Struct. Biol.* 1:213–214.
47. Millett, K., A. Dobay, and A. Stasiak. 2005. Linear random knots and their scaling behavior. *Macromolecules.* 38:601–606.
48. Vologodskii, A., A. V. Lukashin, ..., V. V. Anshelevich. 1974. The knot problem in statistical mechanics of polymer chains. *J. Exp. Theor. Phys.* 39:1059–1063.
49. Koniaris, K., and M. Muthukumar. 1991. Self-entanglement in ring polymers. *J. Chem. Phys.* 95:2873–2881.
50. Rybenkov, V. V., N. R. Cozzarelli, and A. V. Vologodskii. 1993. Probability of DNA knotting and the effective diameter of the DNA double helix. *Proc. Natl. Acad. Sci. USA.* 90:5307–5311.
51. Deguchi, T., and K. Tsurusaki. 1994. A statistical study of random knotting using the Vassiliev invariants. *J. Knot Theory Its Ramifications.* 3:321–353.
52. Katritch, V., W. K. Olson, ..., A. Stasiak. 2000. Tightness of random knotting. *Phys. Rev. E Stat. Phys. Plasmas Fluids Relat. Interdiscip. Topics.* 61:5545–5549.
53. Dobay, A., J. Dubochet, ..., A. Stasiak. 2003. Scaling behavior of random knots. *Proc. Natl. Acad. Sci. USA.* 100:5611–5615.
54. Micheletti, C., D. Marenduzzo, ..., D. W. Sumners. 2008. Simulations of knotting in confined circular DNA. *Biophys. J.* 95:3591–3599.
55. Darcy, I. K., and D. W. Sumners. 1997. A strand passage metrics for topoisomerase action. In *Knots '96: Proceedings of the Fifth International Research Institute of Mathematical Society of Japan*. S. Suzuki, ed. World Scientific, pp. 267–278.
56. Flammini, A., A. Maritan, and A. Stasiak. 2004. Simulations of action of DNA topoisomerases to investigate boundaries and shapes of spaces of knots. *Biophys. J.* 87:2968–2975.